Evidence of Two-Stage Magnetic Reconnection in the 2005 January 15 X2.6 Flare

Pu Wang[1], Yixuan Li[2], Mingde Ding[1], Haisheng Ji[3,4], Haimin Wang[2]

1. Department of Astronomy, Nanjing University, Nanjing, 210093, China
2. Space Weather Research Laboratory, New Jersey Institute of Technology, Newark, NJ 07102
3. Key Laboratory of Dark Matter and Space Science, Chinese Academy of Sciences, Nanjing, 210008
4. Purple Mountain Observatory, Chinese Academy of Sciences, Nanjing, 210008

Abstract

We analyze in detail the X2.6 flare that occurred on 2005 January 15 in the NOAA AR 10720 using multiwavelength observations. There are several interesting properties of the flare that reveal possible two-stage magnetic reconnection similar to that in the physical picture of tether-cutting, where the magnetic fields of two separate loop systems reconnect at the flare core region, and subsequently a large flux rope forms, erupts, and breaks open the overlying arcade fields. The observed manifestations include: (1) remote Hα brightenings appear minutes before the main phase of the flare; (2) separation of the flare ribbons has a slow and a fast phase, and the flare hard X-ray emission appears in the later fast phase; (3) rapid transverse field enhancement near the magnetic polarity inversion line (PIL) is found to be associated with the flare. We conclude that the flare occurrence fits the tether-cutting reconnection picture in a special way, in which there are three flare ribbons outlining the sigmoid configuration. We also discuss this event in the context of what was predicted by Hudson, Fisher, & Welsch (2008), where the Lorentz force near the flaring PIL drops after the flare and consequently the magnetic field lines there turn to be more horizontal as we observed.

Keywords: Sun: corona, Sun: flares, Sun: activity, Sun: magnetic fields
PACS: 96.60.Q, 96.69.lv

1. Introduction

There are a number of models that can explain some aspects of observed properties of solar flares. One way or the other, most flare models still contain a key component of Kopp-Pneuman's original theory to explain two-ribbon flares: flare ribbon emissions are due to magnetic reconnection of overlying arcade fields that are opened by the erupting flux ropes, and the ribbons move away from the magnetic polarity inversion line (PIL) as successive reconnections occur at higher and higher latitudes (Kopp & Pneuman 1976). This and modified models of this kind tend to predict that photospheric magnetic fields do not change after flares. However, more and more evidence demonstrates that photospheric magnetic fields can have permanent changes after flares (Cameron & Sammis 1999, Kosovichev & Zharkova, 2001; Wang et al. 1994, 2002, 2004a,b; Liu et al. 2005, Sudol & Harvey 2005). It is noticeable that building on Kopp-Pneuman scenario, many recent models of flares/CMEs exhibit signatures of two-stage magnetic reconnection. Taking the well received break-out model (Antiochos et al. 1999) as an example, the flares/CMEs occur in multipolar topologies in which reconnection between a sheared arcade and neighboring flux systems triggers the eruption, and this initial external reconnection could be related to remote brightenings (Liu et al. 2006). Another instance is the tether-cutting model, which was proposed by Moore & Labonte (1980) and further elaborated by Moore et al. (2001). This is one of the very few models that imply that the near-surface magnetic fields could have flare-associated changes, and it also proposes a two-step reconnection leading to flares/CMEs. At the eruption onset, the first stage reconnection near the solar surface produces a low-lying shorter loop across the PIL and a longer twisted flux rope connecting the two far ends of a sigmoid. The second stage reconnection begins when the formed twisted rope subsequently becomes unstable and erupts outward, distending the larger scale envelope field that overarches the sigmoid. The opened legs of the envelope field subsequently reconnect back to form an arcade structure and the ejecting plasmoid escapes as a CME. The tether-cutting model may potentially explain other observational facts including: (1) Transverse magnetic fields at flaring PIL increase rapidly following flares (Wang et al. 2002, 2004a); (2) Penumbral decay occurs in the outer border of δ configuration, indicating that the peripheral field lines turn more vertical after flares (Liu et al. 2005; Wang et al. 2004b); (3) Multiwavelength including hard X-ray signatures of preflare activities develop prior to the impulsive phase

of flares (Fárník et al. 2003 and references therein); (4) Hard X-ray (HXR) images show a change of the source morphology from a confined footpoint structure to an elongated ribbon-like structure after the flare maximum (Liu et al. 2007).

Recently, the two-stage nature of magnetic reconnection involved in major flares is further evidenced by observational studies. Xu et al. (2010) presented HXR observations of the 2003 October 29 X10 flare obtained with the Reuven Ramaty High Energy Solar Spectroscopic Imager (RHESSI) (Lin et al. 2002), and identified two pairs of HXR conjugate footpoints at the flare early impulsive phase that are shown to have different temporal evolutions. By carrying out magnetic sequence analysis, Qiu (2009) made a comprehensive study of the 2004 November 7 X2.0 flare and revealed that the flare ribbons first spread along then separate away from the PIL. Guo et al. (2008) and Cheng, Ding, & Zhang (2010) found reconnection and brightening in the core field followed by the final eruption for the 2006 December 13 flare and the 2008 April 26 CME/flare, respectively. All these results strongly suggest that two distinctively separate reconnection processes could occur in succession during a single event. A theoretical progress in the study of magnetic reconnection made by Cassak et al. (2006) shows that slow and collisional reconnection in sheared magnetic fields in the corona can exist for a long time. When the dissipation region becomes thinner and the resistivity drops below a critical value, fast, collisionless reconnection sets in abruptly, increasing the reconnection rate by many orders of magnitude in a very short time. It is possible that the contracting phase of flares, which is observed to be correlated with rapid unshearing and abnormal temperature structures of hard X-ray looptops of a number of flares (e.g., Ji et al. 2006; Shen et al. 2008), corresponds to the first stage, while the ribbon expansion corresponds to the second stage.

However, from the viewpoint that observations and models should yield the same conclusions in all aspects, results reported in the literature thus far have not yet converged especially regarding how the observed changes of photospheric magnetic fields due to flares could reconcile in the two-stage magnetic reconnection scenario, and more importantly, could be understood in the context of coronal magnetic field restructuring. Thus further investigation of individual events should be accumulated to advance our understanding of flaring processes.

In this paper, we study the 2005 January 15 X2.6 flare that was well observed by the Big Bear Solar Observatory (BBSO), with a focus on the flare

ribbon dynamics and the flare-related photospheric magnetic field changes. For this event, Liu et al. (2010) reported an asymmetric filament eruption. The asymmetric filament eruption is a kind of eruption with one point fixed and flare brightening propagates along the PIL together with the expansion/separation from the (PIL), as reported by Tripathi et al. (2006). For this event, Liu et al. (2010) found that magnetic reconnection proceeds along the PIL toward the regions where the overlying field decreases with height more rapidly. Our main goal here is to provide further evidence reflecting physical properties of the two-stage magnetic reconnection, especially, the physical mechanisms for initiating the filament eruption. In § 2 we introduce the data sets used in this study. We present the main results of observations and modeling in § 3, which are summarized and further discussed in § 4.

2. Observations and Data Processing

The source active region, NOAA 10720, produced many X-class flares in 2005 January, and its magnetic configuration and long-term evolution have already received attention in some studies (e.g., Zhao & Wang 2006; Zhao et al. 2008; Wu et al. 2009; Martinez-Oliveros & Donea 2009). As BBSO routinely monitors the activity of the solar chromosphere, the X2.6 flare of January 15 that peaked at 23:02 UT in the GOES soft X-ray flux was fully covered by its full-disk Hα observation with a cadence of 1 minute and a pixel scale of $\sim$ 1 arcsec. Moreover, vector magnetograms were obtained by the Digital Vector Magnetograph (DVMG) system at BBSO with a field of view of about $300'' \times 300''$ targeted at this active region. The hardware of DVMG, consisting of a 1/4 Å band pass filter, a 12-bit 1024 $\times$ 1024 CCD camera, and three liquid crystals acting as polarization analyzers, has been described in detail by Spirock et al. (2002). Each complete set of Stokes data has typically a 1 minute cadence and comprises four images: 6103 Å filtergram (Stokes I), line-of-sight magnetogram (Stokes V), and the transverse magnetogram (Stokes U and Q) (Wang et al. 2002). For each of Q, U, V, we use about 4 second of integration. The pixel scale of vector data is $\sim$ 0.6 arcsec after rebinning to increase the sensitivity of the magnetograms, which is approximately 2 and 20 Gauss for the line-of-sight and transverse magnetic fields, respectively (Spirock et al. 2002, Wang et al. 2002). To fully utilize the vector magnetograms, we resolved the 180° azimuthal ambiguity in the transverse fields by using the "minimum energy" method (Metcalf et al. 2006) and removed the projection effects by transforming the observed

vector magnetograms to heliographic coordinates.

To understand the relationship between the evolution of magnetic fields and primary energy release sites, we use the time profiles as well as images of HXR emissions taken by RHESSI. Aligning images from different sources has been a challenging task. We use the pointing information of the RHESSI instrument, and align the BBSO data with the line-of-sight magnetograms from the Michelson Doppler Imager (MDI) on board the Solar and Heliospheric Observatory by feature matching, the accuracy of which is estimated to be ~ 5 arcsec.

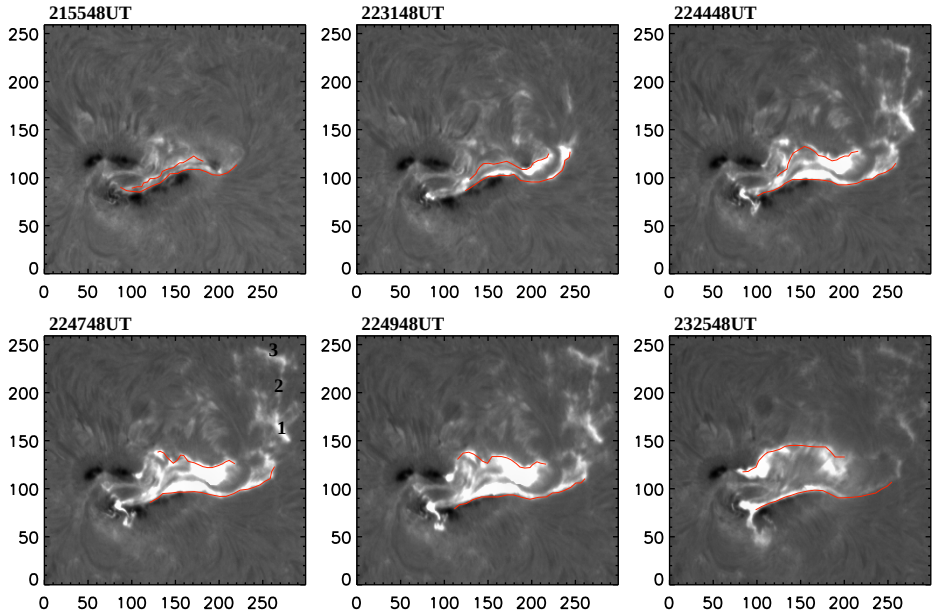

Figure 1: Time sequence of Hα images of the 2005 January 15 X2.6 flare. Three remote brightenings under discussion are marked as 1, 2 and 3. The images are centered on the point (80 arcsec, 350 arcsec) with solar west to the right and north up. The field of view is ~ 320 arcsec $\times \sim 260$ arcsec. The ribbons' moving fronts are marked by the over-plotted lines.

3. Observational Analysis

3.1. Flare Remote Brightening

Although flare energy release may mainly stem from its core emission, study of large-scale structure of flares can help to better understand the

magnetic topology of flaring active region. In a previous work, Liu et al. (2006) summarized the studies of remote brightening, which can be primarily due to hot particles traveling from the flare core to a remote site along large-scale magnetic field lines (e.g., Tang & Moore 1982, Kundu et al. 1983; Nakajima et al. 1985; Hanaoka 1999). In this case, remote brightening can be an important tracer for such a large-scale magnetic field connecting the flare core and the distance place, which is also substantiated by the finding of subsequent formation of transient coronal holes (dimmings) above the remote brightening regions (Manoharan et al. 1996). In some other cases, remote brightenings can be interpreted as disturbances propagating outward from the flare site in the form of Moreton waves (Moreton & Ramsey 1960; Uchida 1974a,b). Observational analyses of remote brightenings have been advanced in recent years. Balasubramaniam et al. (2005) researched them as sequential chromospheric brightenings, which are observed to travel from the flare site outwards. Liu et al. (2006) made a detailed study of an X-class flare and found close correlation as well as difference among flare initiation, Moreton wave, coronal dimming, and remote brightening. In short, no matter which way we look at the remote brightenings, they have been considered as the consequence of eruption that spreads toward the non-flaring regions.

Figure 1 shows the time sequence of Hα images across the flaring interval of the present event. Besides the two prominent flare ribbons, remote brightenings and their northward propagation are very evident. Three of the strongest patches are labeled as 1, 2, and 3 (see the image at 22:47:48 UT). What is striking is that the remote brightenings were launched 5–10 minutes *before* the peak of HXR emission, which can be unambiguously recognized in Figure 2, where we compare the time profile of the H_α intensity of the three patches to that of the HXR emission. With the ordinary remote brightenings in mind, this unusual temporal property leads us to suspect that these Hα emitting patches have different physical implication and could stand for footpoints corresponding to the initial stage of magnetic reconnection with respect to the subsequent onset of main flare HXR emissions.

In order to shed more light on the role of the remote brightenings, we trace the position of a section of the main flare ribbon that has the highest speed of separation motion away from the flaring PIL. This speed is closely associated with the magnetic reconnection rate of flares. Forbes & Priest (1984) supplemented the classical flare model with a quantitative estimation of the magnetic reconnection rate in the coronal reconnecting current sheet (RCS) from observable quantities, i.e., $\varphi_{\rm rec} = \int V_r B_n dl = \partial/\partial t \int B_n da$,

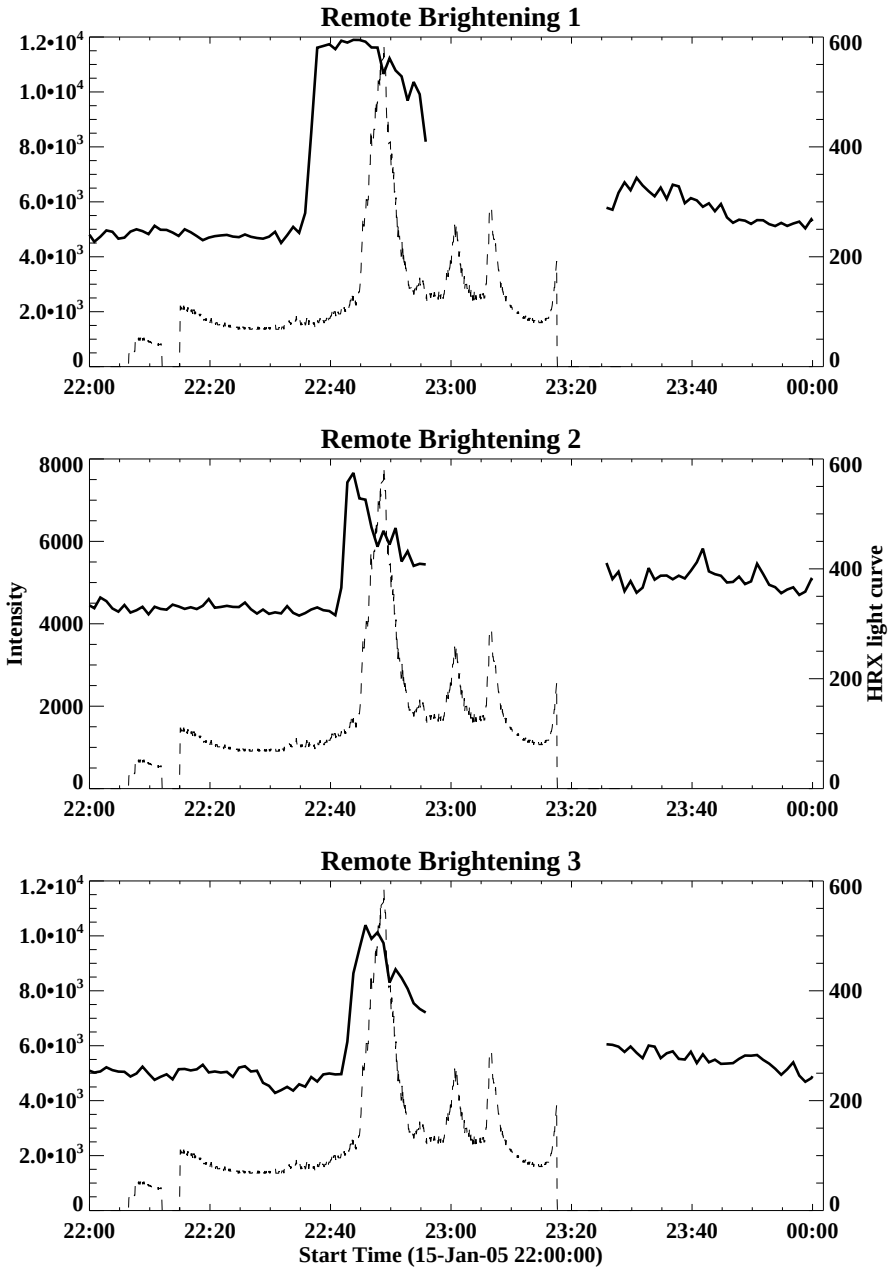

Figure 2: Time profile of the H_α (bandwidth: 0.25 Å) intensity (thick lines) of the three remote brightenings as marked in Fig. 1, with RHESSI 100–300 keV HXR light curve overplotted (dashed lines). It is obvious that the Hα remote brightenings occurred 5–10 minutes before the main HXR phase of the flare, which suggests that they may be footpoints corresponding to the first stage of reconnection.

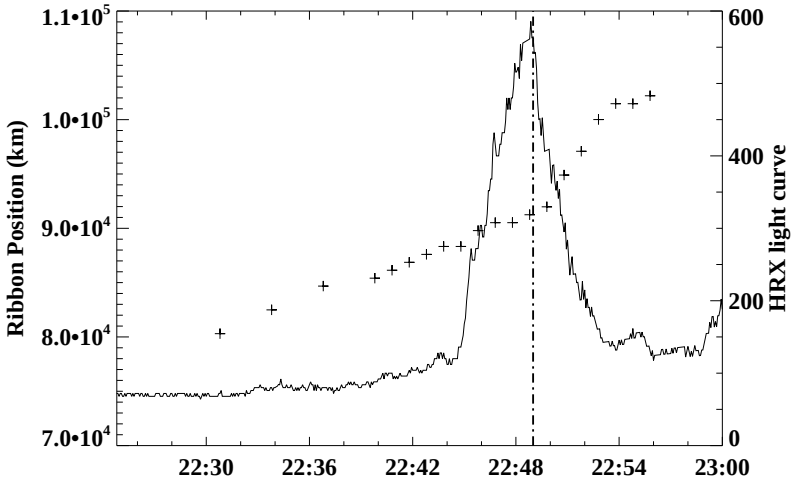

Figure 3: Position of fastest moving ribbon as a function of time ("+"), in comparison with 100–300 keV RHESSI HXR light curve. Two stages of ribbon separation motion are evident, as marked by the vertical dash-dot line.

where V_r is the ribbon separation velocity, B_n is the normal component of the local magnetic field strength measured in the ribbon location, dl is the length along the ribbons, and da is the newly brightened area swept by the flare ribbons. In particular, $E = V_r B_n$ is the convective electric field, often taken as a measure of a reconnection rate. We plot in Figure 3 the ribbon position as a function of time, which clearly shows two stages of ribbon motion: the slower motion (8 km s^{-1}) from ∼22:30–22:49 UT and a faster motion (33 km s^{-1}) from ∼22:49–22:54 UT. This can also be seen in Figure 4 in Liu et al. (2010). There is a slight difference in the timing of the two stages shown in their paper and the present paper. Changing from stage one to two appears at 22:45 UT in Liu et al. (2010) and 22:49 UT in the present paper. The difference is due to that they used kernels (centroid), while we used the front edge. Based on the timing of the HXR emission, a conclusion can be readily drawn that all the Hα remote brightenings occurred before the fast reconnection phase and hence belong to the first stage of the eruption. Later on (see the image at 23:25:48 UT), loops of an arcade are seen overlying the active region, similar to what was observed as a result of sigmoid eruption (e.g., Liu et al. 2007) .

For Figure 3, what we mean is that we can divide the whole flaring period

into two phases according to the different speed of the ribbons front edge before and after 20:49, in the revised reversion of Figure 3.

3.2. Permanent Changes of Photospheric Magnetic Fields After the Flare

The irreversible changes of magnetic fields after flares is a solid observational phenomenon that has been identified for many events. Over a decade ago, the BBSO group discovered rapid and permanent changes of the photospheric vector magnetic fields associated with flares (Wang 1992; Wang et al. 1994; Cameron & Sammis 1999), which have already been confirmed by recent observations. Kosovichev & Zharkova (2001) studied high resolution MDI magnetogram data of the 2000 July 14 "Bastille Day Flare" and located regions with permanent decrease of magnetic flux, which were related to the release of magnetic energy. Using 1 minute cadence GONG data, Sudol & Harvey (2005) surveyed rapid and permanent changes of the line-of-sight magnetic fields that are indeed associated with almost all the X-class flares studied. Earlier, the BBSO group published a number of papers describing the sudden appearance of unbalanced magnetic flux that is associated with flares (Spirock et al. 2002; Wang et al. 2002; Yurchyshyn et al. 2004). All these observations indicate that flaring process, due to its magnetic nature, has a direct observable impact down to the photosphere.

More recently, they presented a new observational result of rapid changes of sunspot structure associated with a substantial fraction of flares (Wang et al. 2004b; Deng et al. 2005; Liu et al. 2005; Chen et al. 2007). In particular, Liu et al. (2005) studied the relationship between the change in δ spot structures and associated major flares for seven events. The results are quite consistent for all the events: part of the penumbral segments in the outer δ spot structure decays rapidly after major flares; meanwhile, the umbral cores and/or inner penumbral regions around the flaring PIL become darker. The rapid changes, which can be identified in the time profiles of white-light mean intensity, are permanent, not transient, and thus are not due to flare emission. To explain these observations, Liu et al. (2005) proposed a reconnection picture in which the two components of a δ spot become strongly connected after the flare. The penumbral fields change from a highly inclined to a more vertical configuration, which leads to penumbral decay. The penumbral region near the flaring PIL becomes darker as a result of increasing transverse magnetic field components.

We have excellent coverage of vector magnetic field observation to study this event in detail. Figure 4 shows a preflare vector magnetogram taken at

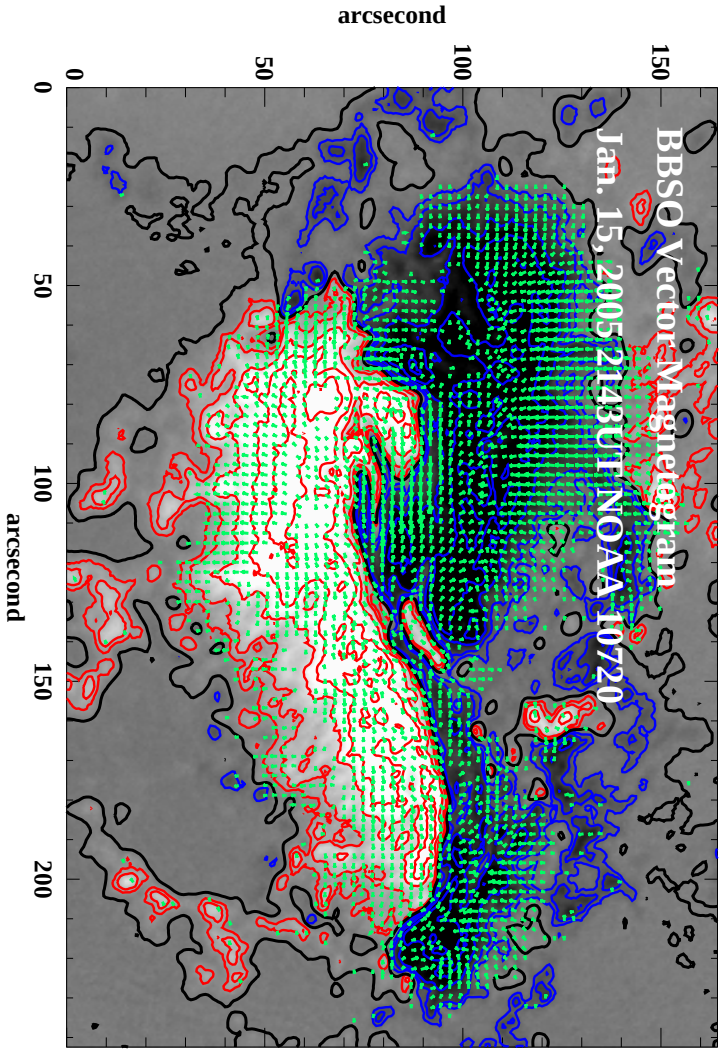

Figure 4: A BBSO vector magnetogram at 2005 January 15 21:43 UT before the X2.6 flare. Green arrows indicate the transverse fields. Red and blue contours are for negative and positive line-of-sight magnetic field strength, respectively. The thick, solid black lines are the PILs of the line-of-sight magnetic field.

21:43 UT. The X2.6 flare mainly occurred in the tongue-shaped west part of the active region, where there are strongly sheared magnetic fields involving long-term flux emergence (e.g., Zhao et al. 2008). By examining a time-lapsed movie compiled using transverse field strength, we immediately identified the location of flare-related enhancement of transverse field strength at the flaring PIL. To illustrate this we show in Figure 5 (bottom panel) the difference map of transverse field between the pre- and postflare states, and plot in Figure 6 the transverse field strength and the corresponding mean inclination angle as a function of time for the most prominently enhanced area (pointed by the arrow in Fig. 5). We find that after the flare the mean transverse field suddenly increased from 450 to 550 Gauss in a section of PIL connecting HXR footpoint emissions, and the mean inclination angle decreased about by 5 degrees accordingly. Furthermore, this pronounced enhancement of transverse field at the flaring PIL most probably started in the first stage of reconnection as discussed in § 3.1 (cf. Figs. 2, 3, and 6). We note that this kind of enhancement can be explained in one of two ways: Either there is a rapid new flux emergence after flares (Wang et al. 2002), or the connectivity at flaring PIL is enhanced after flares. For this event, the former explanation can be rejected due to lack of evidence of increase of line-of-sight flux right after the flare. On the other hand, the latter explanation could be linked to the change of magnetic connectivity in the first phase of the two-stage reconnection, which will be discussed in § 4.

4. Conclusion and Discussions

In this paper, we have presented a multiwavelength study of the 2005 January 15 X2.6 flare that shows intriguing remote brightenings and transverse field enhancement. We here argue that our results provide several pieces observational evidence of the two-stage tether-cutting reconnection mechanism, and we summarize our interpretations as follows:

1. The finding of the remote brightenings that occur early in the event well before the flare main HXR emissions signifies the beginning of the reconnection between magnetic elbows of the sigmoid. The remote brightening areas appear as a special flare ribbon, and together with the ribbons at the flare core region, outlines the overall sigmoidal configuration.
2. Flare ribbon separation started with a slow phase co-temporal with remote brightenings (the first stage of reconnection), and followed by a

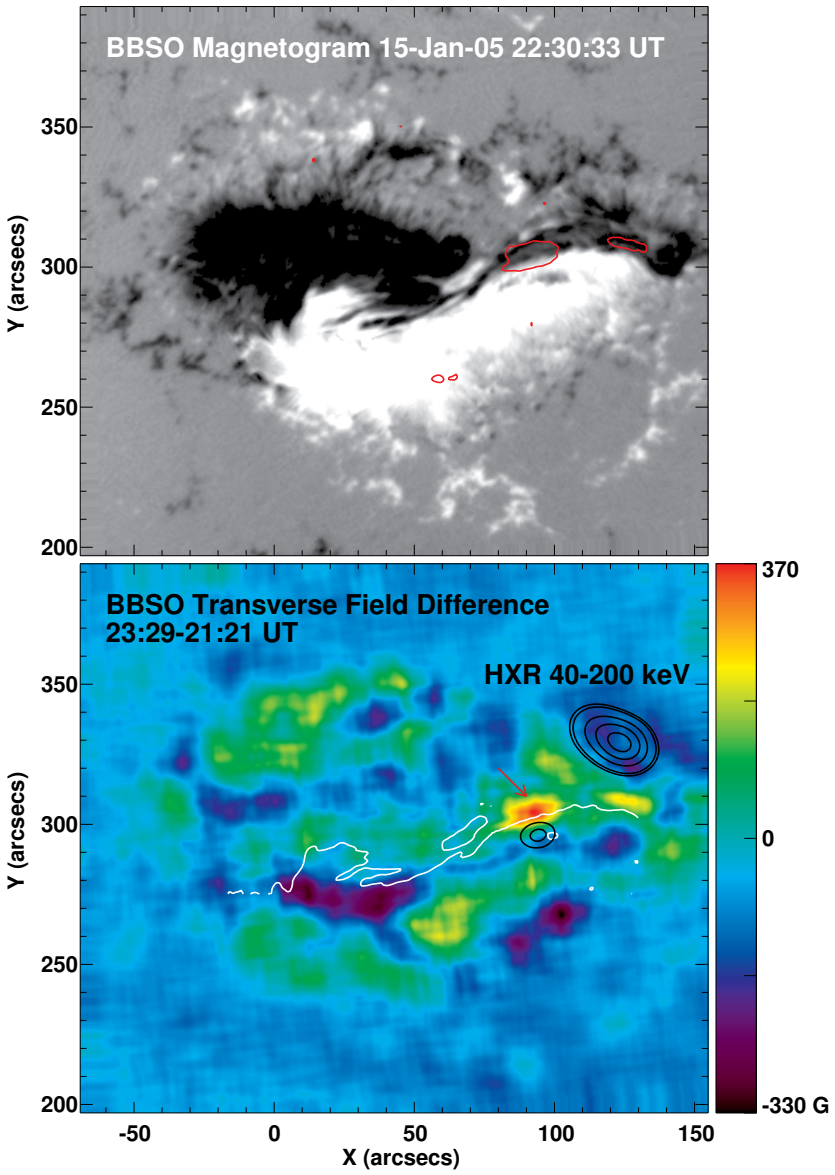

Figure 5: Top: BBSO Line-of-sight magnetogram before the X2.6 flare. Bottom: Difference map of transverse field strength before and after the flare. Regions in *red* indicate an increase of transverse field, with the most prominent area pointed by an arrow. The strongly enhanced regions are also outlined and superposed in the top panel. The cleaned RHESSI image was reconstructed using detectors 3–8 (9.8 arcsec FWHM resolution) and 60 seconds integration time centered on 22:49:18 UT and is shown as contours at levels of 25%, 30%, 50%, 70%, and 90% of the maximum flux. The white line denotes the main PIL of this δ spot.

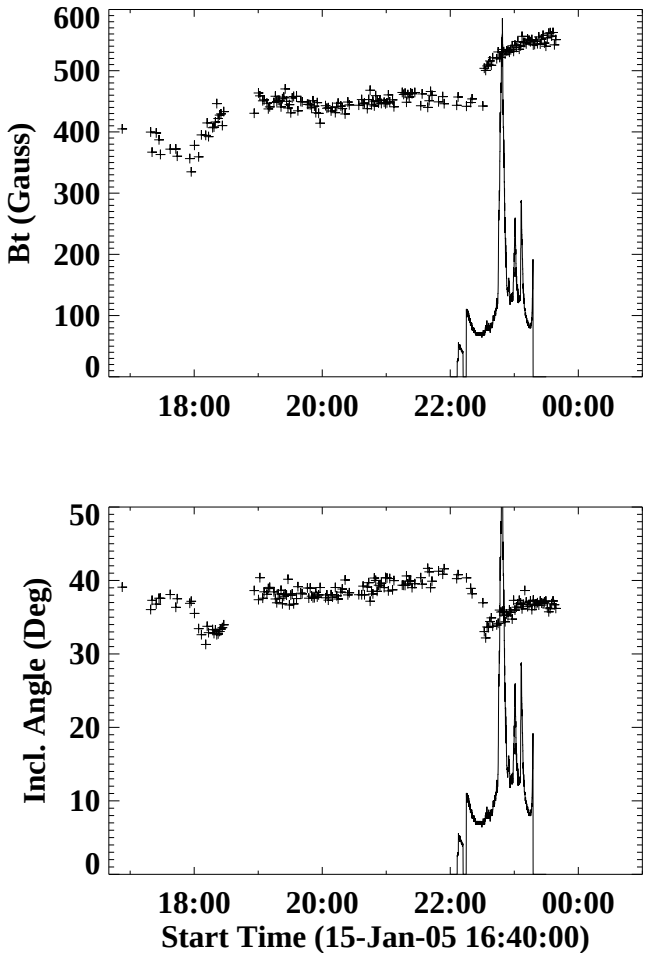

Figure 6: Transverse field strength (top) and corresponding inclination angle (bottom) as a function of time for the arrow pointed region in Fig. 5. The 100–300 keV HXR light curve is overplotted. The mean transverse field strength suddenly increased from 450 to 550 Gauss in a section of PIL connecting HXR footpoint emissions; meanwhile, the mean inclination angle decreased about 5 degrees.

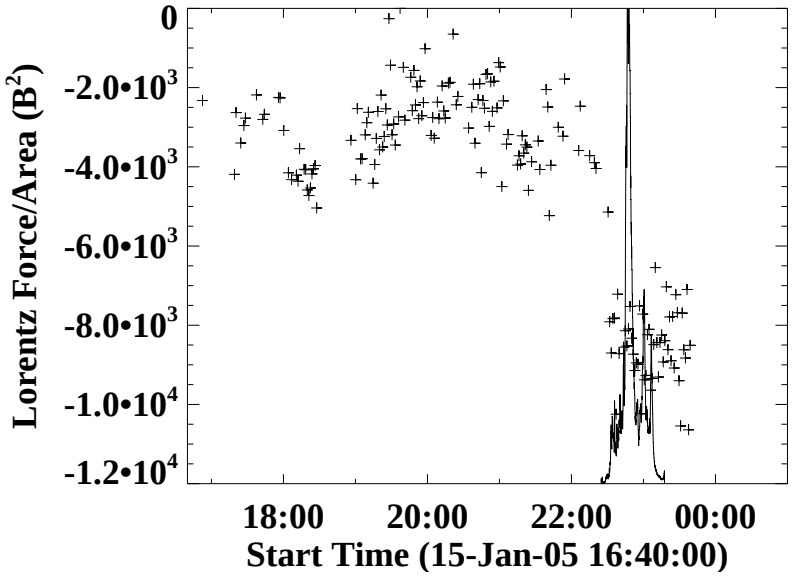

Figure 7: The change of Lorentz force per unit area in the region pointed by arrow in Fig. 5, which has the strongest transverse field enhancement after the flare.

fast phase when HXR emissions peaked (the second stage of reconnection). This two-stage magnetic reconnection accounting for the sigmoid-to-arcade transformation is discernible in Hα images.

3. The significant enhancement of transverse magnetic fields within a region that is beneath the HXR producing flaring loops strongly supports the formation of low-lying field lines as a result of the reconnection. By this way, the observed rapid and permanent transverse field change can be naturally incorporated into the two-stage reconnection scenario.

For this event, Liu et al. (2010) only considered torus instability for this event, because there was a continuous flux emergence in the region (Zhao et al. 2008). With above evidences in mind, we argue that tether-cutting reconnection mechanism to be the most appropriate.

We note that some of our findings are in agreement with the physical picture of Hudson, Fisher & Welsch (2008, hereafter HFW08), who quantitatively assessed the back reaction on the photosphere and solar interior by the coronal field evolution required to release flare energy. More specifically, we found that the postflare photospheric fields become more horizontal. Based

on the study of sudden motion of sunspot (Anwar et al. 1994), HFW08 also introduced the concept of "jerk" produced by coronal restructuring, which may be linked to seismic waves found in powerful impulsive flares (Kosovichev & Zharkova 1998) as suggested by further evidence (e.g. Martinez-Oliveros & Donea 2009). As related to the evolution of vector magnetic fields, HFW08 shows that the near surface Lorentz force should have a sudden drop associated with flares. In their paper, they derived the change of Lorentz force in the form of

$$\delta f_z = (B_z \delta B_z - B_x \delta B_x - B_y \delta B_y)/4\pi \ .$$

Wang & Liu (2010) surveyed over 20 X-class flares and provided direct and indirect evidence of field line changes to more horizontal topology after eruptions. To compare the estimation made by HFW08 with observations of the flare in the current study, we show in Figure 8 the mean change of Lorentz force per unit area as a function of time for the area pointed by the arrow in Figure 5. Indeed, the Lorentz force has an irreversible and sudden change associated with the flare, with a drop of magnitude of 6000 dynecm^2. Integrating over the area of interest yields a change of Lorentz force of 1.0×10^{22} dyne consistent with what was approximated in HFW08. It is possible that this kind of sudden loss of balance may be responsible for the excitation of seismic waves.

Unfortunately, there has no report of seismic wave for this particular event due to lack of Doppler observations. Martinez-Oliveros & Donea (2009) studied an X1.2 flare accompanied by well-observed seismic waves, which occurred 20 hours earlier in the same active region. It is demonstrated that the flare is located in the same site as the X2.6 flare in this study. These will motivate future studies to link several aspects of flares, such as two-stage reconnection, rapid change of magnetic fields, loss of force balance, and excitation of seismic waves, towards a full understanding of the flaring phenomenon.

The authors are grateful to the anonymous referee for his/her valuable comments to improve the paper. We thank Dr. Chang Liu for the discussions and his help for figures in this paper. The authors thank the teams of BBSO, RHESSI, and SOHO for efforts in obtaining the data. This work was supported by NSF grants AGS-0839216 and AGS-0849453, NASA grants NNX 08AQ90G and NNX 08AJ23G, NSFC grants 10833007, 10933003 and 10928307 and the 973 Program No. 2011CB811402.

References

Antiochos, S. K., DeVore, C. R., and Klimchuk, J. A. 1999, ApJ, 510, 485

Anwar, B., Acton, L. W., Hudson, H. S., Makita, M., McClymont, A. N., and Tsuneta, S., 1993, Solar Phys., 147, 287

Balasubramaniam, K. S., Pevtsov, A. A., Neidig, D. F., Cliver, E. W., Thompson, B. J., Young, C. A., Martin, S. F., and Kiplinger, A. 2005, ApJ, 630, 1160

Cameron, R. & Sammis, I. 1999, ApJ, 525, L61

Cassak, P. A., Drake, J. F. and Shay, M. A. 2006, ApJ, 644, L145

Chen, W., Liu, C., and Wang, H. 2007, ChJAA, 7, 733

Cheng, X., Ding, M. D., Guo, Y., Zhang, J., Jing, J., and Wiegelmann, T. 2010, ApJ, 716, 68

Deng, N., Liu, C., Yang, G., Wang, H., and Denker, C. 2005, ApJ, 623, 1195

Fárník, F., Hudson, H.S., Karlický, M. and Kosugi, T. 2003, A&A, 399, 1159

Forbes, T. G., and Priest, E.R. 1984, Solar Phys., 94, 315

Guo, Y., Ding, M. D., Wiegelmann, T., and Li, H 1998, ApJ, 679, 1629

Hanaoka, Y 1999 PASJ, 51, 483

Hudson, H. S., Fisher, G. H., and Welsch, B.T. 2008, ASP Conference Series, 383, 221

Ji, H., Huang, G., Zhou, T., Li, Y., Zhang, Y., and Song, M. 2006, ApJ, 636, L173

Jing, J., Chen, P. F., Wiegelmann, T., Xu, Y., Park, S. H., and Wang, H. 2009, ApJ, 696, 84

Kopp, R. A. and Pneuman, G. W. 1976, Solar Phys., 50, 85

Kosovichev, A. G. and Zharkova, V. V. 1998, Nature, 393, 317

Kosovichev, A. G. and Zharkova, V. V. 2001, ApJ, 550, L105

Kundu, M. R., Bobrowsky, M., and Rust, D. M. 1983, ApJ, 265, 1084

Lin, R., Dennis, B. R., and Hurford, G. J. et al. 2002, Solar Phys., 210, 3

Liu, C., Deng, N., Liu, Y., Falconer, D., Goode, P. R., Denker, C., and Wang, H. 2005, ApJ, 622, 722

Liu, C., Lee, J., Deng, N., Gary, D. E., and Wang, H. 2006, ApJ, 642, 1205

Liu, C., Lee, J., Jing, J., Liu, R., Deng, N., and Wang, H. 2010, ApJ, 721, L193

Liu, C., Lee, J., Yurchyshyn, V., Deng, N., Cho, K., Karlický, M., and Wang, H. 2007, ApJ, 669, 1372

Martinez-Oliveros, J.C., and Donea, A.C. 2009, MNRAC, 395,39

Manoharan, P. K., van Driel-Gesztelyi, L., Pick, M., and Demoulin, P. 1996 ApJ, 468, L73

Metcalf, T. R., Leka, K. D., Barnes, G., Lites, B. W., Georgoulis, M. K., Pevtsov, A. A., Balasubramaniam, K. S., Gary, G. A., Jing, J., Li, J., Liu, Y., Wang, H. N., Abramenko, V. A., Yurchyshyn, V., and Moon. Y.J. 2006, Solar Phys., 237, 267

Metcalf, T.R. 2008, Solar Phys., 247, 269

Moore, R. L., and Labonte, B. J. 1980, in IAU Symp. 91, Solar and Interplanetary Dynamics, ed. M. Dryer and Ed. Tandberg-Hanssen (Boston: Reidel), 91, 207-210

Moore, R.L., Sterling, A.C., Hudson, H.S., and Lemen, J. 2001, ApJ, 552, 833

Moreton, G. E. and Ramsey, H. E. 1960, PASP, 72, 357

Nakajima, H., Dennis, B. R., Hoyng, P., Nelson, G., Kosugi, T., and Kai, K. 1985, ApJ, 288, 806

Qiu, J. 2009, ApJ, 692, 1110

Shen, J., Zhou, T., Ji, H., Wang, N., Cao, W., and Wang, H. 2008, ApJ, 686, L37

Spirock, T. J., Yurchyshyn, V. B., and Wang, H. 2002, ApJ, 572, 1072

Sudol, J.J. and Harvey, J.W. 2005, ApJ, 635, 647

Tang, F. and Moore, R. L. 1982, Solar Phys., 77, 263

Tripathi, D., Isobe, H., and Mason, H.E. 2006, A&A, 453, 1111

Uchida, Y. 1974a, IAUS, 57, 383

Uchida, Y. 1974b, Solar Phys., 39, 431

Wang, H. 1992, Solar Phys., 140, 85

Wang, H. and Liu, C. 2010, ApJ, submitted

Wang, H., Spirock, T. J., Qiu, J., Ji, H., Yurchyshyn, V., Moon, Y., Denker, C., and Goode, P. R. 2002, ApJ, 576, 497

Wang, H., Ewell, M.W., Zirin, H., and Ai, G. 1994, ApJ, 424, 436

Wang, H., Qiu, J., Jing, J., Spirock, T. J., Yurchyshyn, V., Abramenko, V., Ji, H., and Goode, P. R. 2004a, ApJ, 605, 931

Wang, H., Liu, C., Qiu, J., Deng, N., Goode, P. R., and Denker, C. 2004b, ApJ, 601, L195

Wu, S. T., Wang, A. H., Gary, G. A., Kucera, A., Rybak, J., Liu, Y., Vrsnak, B., and Yurchyshyn, V. 2009, Adv. Space Review, 44, 46

Xu, Y., Jing, J., Cao, W., and Wang, H. 2010, ApJ, 709, L142

Yurchyshyn, V. B., Wang, H., Abramenko, V., Spirock, T. J., and Krucker, S. 2004, ApJ, 605, 546

Zhao, H., Wang, J., Zhang, J., Xiao, C., and Wang, H. 2008, ChJAA, 8, 133

Zhao, M. and Wang, J. 2006, Proc. IAU Symp. 233, 41